Soft Matter

Accepted Manuscript

ROYAL SOCIETY OF CHEMISTRY

www.rsc.org/softmatter

Cite this: DOI: 10.1039/c0xx00000x

www.rsc.org/xxxxxx

Full Paper

Effect of millimetre waves on phosphatidylcholine membrane models: a non thermal mechanism of interaction.

Amerigo Beneduci[*a,b], Katia Cosentino[a], Stefania Romeo[c], Rita Massa[d] and Giuseppe Chidichimo[a,b]

Received (in XXX, XXX) Xth XXXXXXXXX 20XX, Accepted Xth XXXXXXXXX 20XX
DOI: 10.1039/b000000x

The nonthermal biological effects of millimeter waves has been mainly attributed to the interaction with biological membranes. Several data on biomimetic membrane systems seem to support this conclusion. In this paper a mechanistic hypothesis is evaluated to explain such interaction taking into account experimental NMR data on deuterium-labeled phospholipid vesicle. These data showed that millimeter waves induce a time and a hydration-dependent reduction of the water ordering around the phosphocholine headgroupds. This effect is here interpreted as a change in membrane water partitioning, due to the coupling of the radiation with the fast rotational dynamics of bound water molecules, that results in a measurable relocation of water molecules from the inner to the outer binding regions of the membrane interface. When millimeter wave exposure is performed in the vicinity of the transition point, this effect can lead to an upward shift of the membrane phase transition temperature from the fluid to the gel phase. At a macroscopic level, this unique sensitivity may be explained by the universal dynamic behaviour of the membranes in the vicinity of the transition point, where a pretransitional increase of membrane area fluctuations, i.e., of the mean area per phospholipid headgroup, is observed. Exposure to millimeter waves, increases the above fluctuations and enhances the second order character of the transition.

1. Introduction

The use of millimeter waves (MMWs, 30-300 GHz) in wireless communication technology have been considerably increased during the last years, due to the need for high data rate wireless capacities. [1, 2] Although the power density emitted by MMWs sources is below 1 mW/cm^2 and no significant heating has been observed in exposed biological systems,[1,3] different authors claim that low-power millimeter waves may induce important non-thermal biological effects.[1, 4-15]

The hypothesis of a non-thermal mechanism involving biological membranes has been early proposed by Fröhlich (1988),[16] who pointed out that the high electric field (~10^5 V/cm) across the membrane double layer (thickness of the order (0.01 μm), causes strong electric polarization. Membrane elastic oscillations, corresponding to sound wave velocities of the order of 10^5 cm/s, can therefore lead to electric vibrations with frequencies in the range 10-100 GHz, estimated by the ratio between the sound wave velocity and its wavelength equal to one half the membrane thickness. That is, biomembranes can act as oscillating electric dipoles with frequencies in the millimeter wave region. Fröhlich further considered active biological systems as open systems thermally coupled to the environment. The system is open to food (metabolic energy) and other non-thermal energy supplies in order to get stabilized in states (or modes) of oscillations, far from its thermal equilibrium. Modes are coupled by non-linear long-range interactions and at each mode is associated a chemical potential whose value depends on its quantum energy. Fröhlich showed that, when the rate of energy supply, given by the sum of the metabolic energy and of the millimeter wave energy, exceeds a threshold the system is pointed toward a highly coherent state characterized by only one mode of oscillation. This can occur only if dipole vibrations occur in a narrow band of resonance frequencies and the coupling constant between the system components are large enough. Under these conditions, strong long-range dipole-dipole attractive forces, with an interdipole interaction potential proportional to r^{-3}, are established. Bose condensation of the vibrational modes to the lowest frequency oscillation mode leads to a metastable state with net dielectric polarization (coherent excitation).

Recently, Reimers et al. revised Fröhlich's model showing that "weak condensates", that do not require coherence, may be produced by microwave energy and may significantly affect biological systems.[17] However, Fröhlich's theory has not yet been unambiguously proven, even though some studies showed that the growth of some yeast and bacteria cells could be affected by millimeter waves only at specific frequencies, suggesting a resonant interaction mechanism.[4,5,12]

It is worth noting that, even if this would occur, spectral resonances can be hardly tuned due to the water-dominated absorbance of the MMW energy in biological media.[18-19]

In the recent years, membrane modelling and simulations have been increasingly used in order to study wave interaction with

membranes, including the effects of MMWs at a molecular level.[20-29] Exposure at 60 GHz and low power densities (μW/cm^2), significantly affects the lateral pressure of phospholipid monolayer.[20] Significant alterations were also observed on the physical-chemical properties of cell-sized unilamellar vesicles (GUVs) exposed at 53.57 GHz and average SAR of less than 1 W/Kg.[24] Recently, it was shown that wide-band exposure in the 53-78 GHz range affects the membrane permeability to water in GUVs subjected to osmotic pressure.[23] Moreover, in similar exposure conditions, the aging process occurring in large unilamellar vesicles was inhibited.[23] It has been pointed out that millimeter waves may affect the

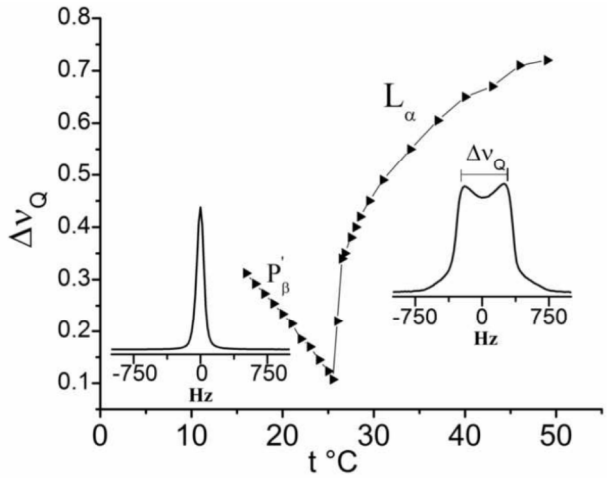

Figure 1. Quadrupole splitting versus temperature across the main phase transition point of a DMPC MLV

membrane-water vesicle interface. This hypothesis has been recently supported by ^{2}H-NMR spectroscopic studies on deuterium-labeled phospholipid vesicles, where MMWs exposure at 53-78 GHz, induced a hydration-dependent reduction of the water ordering at the membrane interface which led to an upward shift of the membrane main phase transition point.[22,29] All the above results have been attributed to non-thermal effects, either because of the use of very low incident power (of the order of several μW) or because the observed effects were opposite to those that would be caused by a thermal increase of the membrane sample. However, so far, no interaction mechanisms have been proposed. Here, we provide an overall picture on the response of 1,2-dimyristoyl-sn-glycero-3-phosphatidylcholine membranes to MMWs over a wide range of temperatures across the main phase transition point, and we suggest a theoretical model that explains for the MMWs induced effects on these biomimetic membrane systems.

2. Experimental

2.1 Sample preparation and NMR acquisition

1,2-Dimyristoyl-sn-glycero-3-phosphatidylcholine (DMPC) was purchased from Sigma Aldrich with a 98.8 % purity and used without further purification. ^2H_2O was obtained from Cambridge Isotope Inc. having a purity of 99.98 %. Multilamellar vesicles (MLVs) were prepared as described elsewhere.[22,29] Briefly, DMPC powder was dried to constant weight in vacuum at room temperature and then hydrated with heavy water to yield multilamellar vesicles (MLVs) containing from 7 up to 11 water moles per mole of lipids (n_w). Samples were prepared with a total weight of about 60 mg per sample in order to have an optimal thickness of about 3 mm in the NMR tube. Deuterium spectra were acquired with a Bruker Avance 300 spectrometer at 46.52 MHz using a phase cycled quadrupole echo sequence with $\pi/2$ = 7 μsec, τ_2 = 50 μsec and a recycle delay of 1 s followed by Fourier transformation. 32 to 128 transients were averaged with a spectral width of 30 KHz. All free-induction decay (FID) were apodized with an exponential multiplication corresponding to a line broadening of 20 Hz. Temperature inside the probe was strictly controlled by the Bruker VT 2000 unit.

2.2 Millimeter wave exposure set up

A detailed description of the MMW exposure set-up was done elsewhere.[19] Briefly, the radiation was generated by a wide-band power source (Amphit-32, MicroMedTech, Nizhny Novgorod, Russia) in the 53.57-78.33 GHz frequency (*f*) range and propagated inside the NMR probe containing the sample, through a diamagnetic metallic circular waveguide terminating with a dielectric antenna. Under this condition, real-time NMR spectra acquisition was allowed, in strictly controlled temperature conditions.

2.3 Curve-Fitting procedure

The iterative nonlinear least squares Levenberg-Marquardt method was used for all curve-fitting procedures. This method involves an iterative improvement of parameter values in order to reduce the sum of the squared errors between the function and the measured data points. At each iteration the parameters used in the model were varied in order to minimize the chi-square χ^2:

$$\chi^2 = \frac{1}{n^{eff} - p}\sum_i w_i\left[y_i - f\left(x_i; p_1, p_2, ...\right)\right]^2$$

where, w_i is a weighting coefficient, y is the dependent variable, x is the independent variables, n^{eff} is the total number of experimental points used in the fitting, p is the total number of adjustable parameters used in the fitting, p_1, p_2,… are the model parameters which are varied in order to minimize χ^2. Standard errors were calculated as, $\sigma_i = (C_{ii}\,\chi^2)^{1/2}$ where C_{ii} is the diagonal element of the variance-covariance matrix.

2.4. Dosimetry

The exposure set-up was made up of a circular waveguide (internal radius of 2 mm), fed at one end by the MMW source and terminated on the other end with a dielectric antenna. In particular, the source was a noise generator: a wide band klystron working in the 53.37-78.33 GHz frequency (*f*) range and with input power varying between 5 μW- 20 μW (being the signal not levelled but stable in time). The dielectric antenna was made up of Teflon, with a radius of 3 mm and height of 40 mm. At the

end of the dielectric antenna the quartz cuvette (internal radius 3 mm, height 15 mm) filled with the sample (3 mm thick) has been modelled. Two saddle coils were also included in the model to simulate the RF coils of the NMR probe where samples were inserted (Supplementary Figure S1A and B).

The power deposition pattern inside the sample was evaluated numerically by using CST Microwave Studio, a commercial code based on the Finite Integration Technique (FIT).

The simulations were carried out at 74 GHz and the electromagnetic parameters were set as in Table 1 (media complex relative permittivities, $\varepsilon = \varepsilon_r' - j\,\varepsilon_r''$, where $\varepsilon'' = \sigma_{eq}/\omega\varepsilon_0$, being $\omega = 2\pi f$ Hz; $\varepsilon_0 = 1/(36\pi \times 10^9)$ F/m).

For the simulation, the region of interest was divided in hexahedral elements; the mesh generation was based both on the material wavelength refinement and on the length based mesh refinement. Therefore, the mesh dimensions of the computing grid inside the sample were 0.3 mm in the vertical direction y, and 0.5 mm in the horizontal directions x and z, in both cases a value below the wavelength inside the sample (λ_m = 1.3 mm at 74 GHz).

Table1 Electromagnetic parameters adopted in numerical simulations

Medium	ε_r'	ε_r''	σ_{eq}
Biological sample	3.8	2.3	9.29
Quartz glass	3.78		
Teflon	2.10		

The mass density of the biological medium was $\rho = 1110$ kg/m^3

The following dosimetric parameters were calculated:[30,31]

- $|E^1(x,y,z)|$: the local electric field amplitude per unit incident power [(V/m)/W]. This was evaluated at each node of the computing domain.
- $SAR^1(x,y,z) = \sigma_{eq}\,|E^1|^2/2\rho$: the local absorbed power per unit mass and per unit incident power [(W/kg)/W]. This is also the local specific efficiency, and it is zero outside the sample (σ_{eq}=0). It is understood that, should the incident power be $P_0 \neq 1$ W, the local absorbed power per unit mass would be P_0 x $SAR^1(x,y,z)$ = SAR (x,y,z) = specific absorption rate [W/kg].
- AV^1: the average $SAR^1(x,y,z)$ over the sample [(W/kg)/W].

3. Background

3.1 Membrane phase transition and deuterium NMR spectroscopy

Multilamellar vesicles (MLVs) are useful biomimetic membrane systems formed by direct hydration of dry phospholipids. Depending on the water/lipid mole ratio, on the phospholipids and on the temperature, different phases (polymorphism) can be generated. Among these, the fluid phase, where lipids are arranged in bilayer structures (lamellae), is generally obtained at temperatures above about 25 °C[22] and is found in biological membranes of cells and cell organelles. The transition from the fluid phase to a more ordered gel phase is called main phase transition, T_m.

Membrane phase transition processes can be studied by wideline NMR spectroscopy on deuterium labeled MLVs such as phospholipid/heavy water systems. The physical observable is the heavy water quadrupole splitting ($\Delta\nu_Q$) that is particularly sensitive to changes of the bilayer structure.[22, 32-35] For unoriented multilamellar samples, $\Delta\nu_Q$ is the distance (Hz) between the principal peaks of the ^{2}H-NMR powder spectra (Fig. 1) and is given by eq. (1):

$$\Delta\nu_Q = \sum_1^n |P_i \Delta\nu_i| = \frac{3}{4}\nu_Q \sum_1^n |P_i S_i| \quad (1)$$

where, P_i is the fraction of water molecules that populates the interface region i contributing a quadrupole splitting $\Delta\nu_i$, ν_Q is the quadrupole coupling constant of heavy water equal to 220 KHz and S_i is a molecular order parameter of water at the interface region i. It brings information on the dynamic processes involved at the membrane/water interface and is therefore sensitive to the membrane phase.

3.2 Pretransitional phenomena in membranes: Landau's theory

In phospholipid/water systems, the main phase transition is a first order process. This can be clearly seen by the discontinuity of the heavy water quadrupole splitting at the transition point (~ 25 °C) between the ordered (gel-ripple phase, P_β') and the fluid phase (L_α) for a DMPC/^2H_2O model membrane (Fig. 1). However, phospholipid membranes show precritical (or pretransitional) phenomena near the transition point, such as nonlinear increase of membrane permeability,[36-38] anomalous swelling,[39-41] and non linear decrease of the heavy water quadrupole splitting (Fig. 1). Precritical phenomena have been described by thermal fluctuations of the orientational order parameter associated to the lipid chains,[42, 43] as well as by fluctuations of the lateral packing density[40] and of the membrane area.[44] Near the transition point, fluctuations increase and this results in a non-linear variation of the membrane response functions. However, the membrane does not reach the critical (or pseudocritical) temperature (T_c) at which the response functions would diverge because the first order transition occurs interrupting the precritical phenomena.[42]

First order phase transitions that exhibit precritical behavior (weakly first order) can be treated with the general theory of Landau as they would be of second order.[42] Landau's theory describes the universal behaviour of many-particle systems near the phase transition, i.e., the decrease of the order parameter as $(T-T_c)^x$ and the increase of the order parameter fluctuations as $|T-T_c|^{-x}$, where $x > 0$ is the critical exponent. All heavy water/phospholipid membrane systems exhibit a reduction of the water quadrupole splitting approaching T_m.[45] This universal behaviour has been explained by the increase of the thermal fluctuations of the area/lipid molecule near the transition point.[45] $\Delta\nu_Q$ (eq. 1), averages to zero value in regions of the bilayer where the membrane area fluctuations exceed a value corresponding to the size of one or a few water molecules.

Landau's theory can be applied to the fluid-order membrane phase transition using $\alpha = A - A_{L\alpha}$ as order parameter for describing the main phase transition, where A is the area per lipid molecule in the plane of the bilayer and $A_{L\alpha}$ the average area in the L_α phase.[45] In the vicinity of the transition point, the Landau free energy variation from the equilibrium (per molecule) is:[41, 45]

$$\delta F = \frac{1}{2} a |T - T_c|^x (1 + \xi^2 q^2) \delta\alpha_0^2 \qquad (2)$$

where, $\delta\alpha_0$ is the amplitude of the deviation of the order parameter α from its equilibrium value, $a > 0$, independent on T, is a coefficient that depends on the chemical-physical properties of the lipid bilayer system, ξ is the coherence length and q is the wave number of the mode of fluctuation.[41] The coherence length determines the extension of the order parameter fluctuations in the membrane plane. While the fluctuations fall off exponentially with ξ, the coherence length increases on approaching the critical point. The coherence length is therefore small for temperatures not close to the critical temperature. Membranes cannot reach their critical point because the critical behaviour is interrupted by the intervening of the first order transition at T_m. Under this assumption, the term $\xi^2 q^2 << 1$ and can be neglected in equation (2).[41, 45]

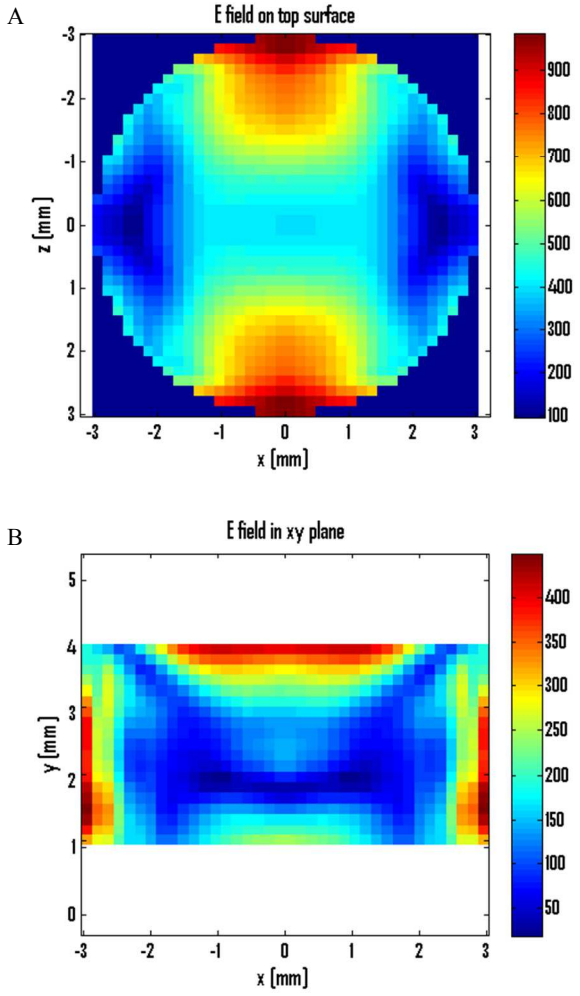

Fig 2 Electric field (V/m) distribution on the transverse (top layer, A) and longitudinal planes (B) of the exposed sample at 74 GHz with 1 W input power.

It follows that, for a mode of fluctuation with $\delta F = kT/2$, the strength of the thermal fluctuations is given by:

$$\delta\alpha_0^2 = \frac{kT}{a} |T - T_c|^{-x} \qquad (3)$$

From the definition of quadrupole splitting of deuterated water (eq. (1)), P_i is the probability of finding a water molecule in the interface region i. This probability is > 0 in regions where the area fluctuations are less than a threshold value, ΔA_0, and is zero when fluctuations exceed it. The probability to have area fluctuations smaller than ΔA_0, is defined by the normalized time-averaged water quadrupole splitting, $\Delta\nu_Q/\Delta\nu_0$, with $\Delta\nu_0$= 1.22 kHz being the quadrupole splitting at high temperatures where no fluctuations occur. Under the assumption that the area-fluctuation energy required to accommodate a water molecule is small compared to kT, the normalized time-averaged splitting is inversely proportional to the amplitude of the area fluctuations:[45]

$$\frac{\Delta\nu_Q}{\Delta\nu_0} = \Delta A_0 \left(\frac{2}{\pi}\right)^2 \left(\frac{a}{kT}\right)^{x/2} |T - T_c|^{x/2} \propto \frac{\Delta A_0}{\delta\alpha_0} \qquad (4)$$

4. Results and Discussion

4.1 Dosimetry

Simulation data demonstrated that, due to the high conductivity (σ_{eq}) of the biological medium, the electric field has its maximum intensity on the surface of the sample (Figure 2A and B). For this reason we have post-processed the obtained numerical results, by using simple Matlab scripts, in order to calculate SAR[1] values for different layers of the sample along the y axis. Each layer is 1 mm thick; the layer 1 identifies the top surface of the samples while the layer 3 is the bottom one. In Table 2 the Average SAR[1] values for the various layers of the sample are reported as well as the average SAR[1] in the whole sample. SAR[1] values are higher on the top of the sample and decrease approaching the bottom layer; the latter is larger than the second layer because of the coupling with the walls of the quartz sample holder. In Table 2 the corresponding SAR in the case of maximum input power (20 μW) is also reported and a power density of about 3 μW/cm^2 can be estimated.in the top layer.

The SAR levels are in all cases much lower than 1.6 W/kg, the currently accepted safety limits as defined by the International Commission on Non Ionizing Radiation Protection.[46]

Table 2 Average SAR values for different layers (1 mm thick) of sample 3 mm thick in case of 1W and 20μW of input power

f [GHz]	Layers	AV[1] (W/kg)/W	AV[1] (whole sample) (W/kg)/W	SAR (mW/kg) 20 μW input power
74	1 (top)	1246	715	24.9
	2 (middle)	364		7.3
	3 (bottom)	445		8.9

4.2 Macroscopic interpretation of the non-thermal membrane/MMW interaction

Data on the normalized splitting of the DMPC/^2H_2O multilamellar sample show that 4h of MMWs exposure induces a decrease of the water quadrupole splitting in the fluid phase and

Table 3 Fitting results of the normalized splitting by eq. (4).

DMPC-^2H_2O	T_c(°C)	$x/2$	$a \times 10^4$ (JK^{-x}Å^{-4})	ΔA_0 (Å^2)	χ^2
Sham $L_\alpha \rightarrow P_{\beta'}$	23.8 (0.2)	0.49 (0.04)	1.50 (0.03)	7.6 ± 0.1	1×10^{-5}
$P_{\beta'} \rightarrow L_\alpha$	27.2 (0.3)	0.46 (0.02)	2.50 (0.04)	13 ± 2	5×10^{-6}
MW $L_\alpha \rightarrow P_{\beta'}$	24.8 (0.2)	0.51 (0.03)	0.60 (0.01)	6.5 ± 0.8	1×10^{-4}
$P_{\beta'} \rightarrow L_\alpha$	30.1 (0.6)	0.48 (0.02)	0.70 (0.06)	12 ± 2	7×10^{-6}

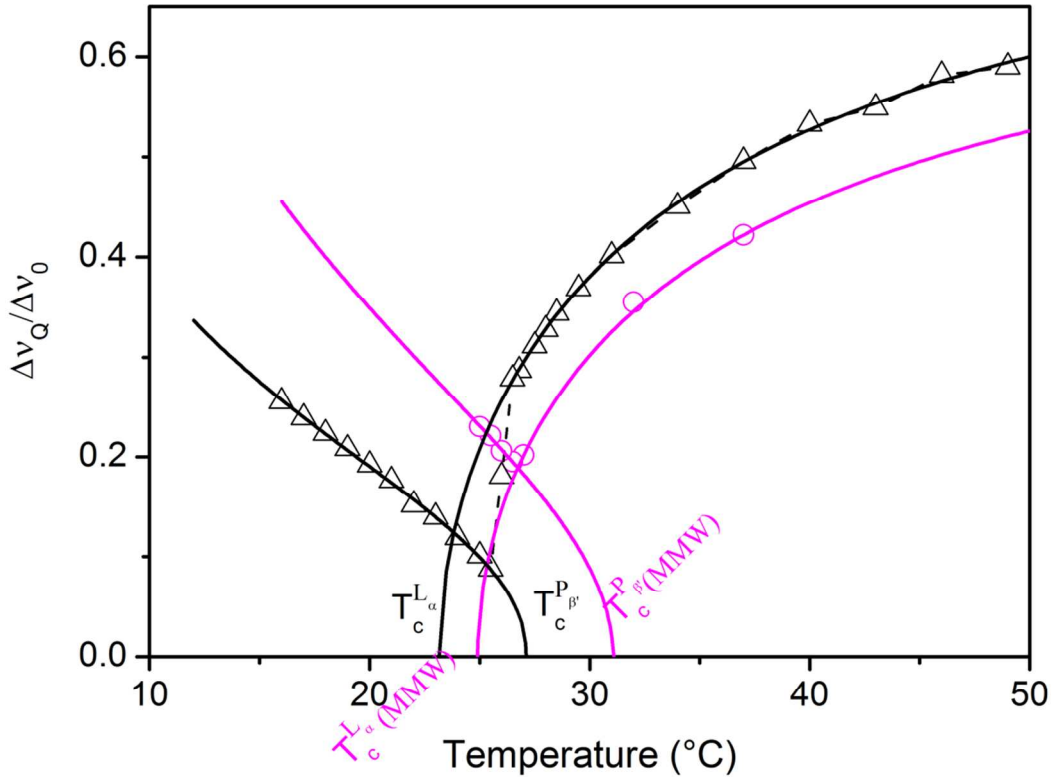

Fig. 3 Effect of the 53-78 GHz wideband exposure on the normalized splitting across the membrane phase transition. Under mm-wave exposure (●), the change of the order parameter of water in DMPC-^2H_2O (n_w = 11) at T_m is less pronounced and the transition temperature is shifted upward compared to the unperturbed, sham exposed membrane (■). Points are the means of three independent experiments and the error bars are contained within the symbols. The solid lines are the best fits of the data performed by eq. 4 (Table 1). The critical temperatures for the fluid-to-ordered phase transition process and those for the reverse process, are respectively indicated by the following symbols $T_c^{L\alpha}$ and $T_c^{P\beta'}$ for the sham exposed sample and $T_c^{L\alpha}$(MMW) and $T_c^{P\beta'}$(MMW) for the millimeter wave exposed sample.

an increase in the ordered phase as compared to the sham exposed sample (Figure 3). At the transition point a reduction of the quadrupole splitting discontinuity occurs and an upward shift of the transition temperature of about 1.5 °C, is induced. Based on the membrane fluctuation model, experimental data points were fitted with equation (4) by freely varying all the model parameters, in order to minimize the χ^2. The results, summarized in Table 3, were used to build up the fitting curves displayed in Figure 3. In agreement with the theory,[41] as well as with previous experimental data,[45] the critical exponent was, in all cases, fitted close to 0.5 (i.e. x = 1). As predicted by the area fluctuation model, the values of ΔA_0 were close to the van der Waals area of one water molecule, 6.16 Å^2.[47, 48] Moreover, the critical temperatures calculated here for the sham exposed membrane (Table 3) are in good agreement with values from literature for the same DMPC system.[45] MMW exposure induces an upward shift of the critical temperature of the fluid-to-gel phase transition, from 23.8 to 24.8 °C (Table 3), which is very close to the main phase transition temperature (25.5 °C).

Large differences are found also in the value of the coefficient a. This can be interpreted as the specific heat for membrane area fluctuation (for x = 1). In exposed membranes a decreases down to 1/3 of the value in the control system (Table 3) meaning that, next to the phase transition, a much lower thermal contribution is required to get fluctuations of the polar head mean area. To support this hypothesis the dependence of the strength of membrane area fluctuation ($\delta\alpha_0^2$) on the temperature is displayed in Figure 4. The displayed curves were calculated by equation (3) using the parameter values reported in Table 3. Under MMW exposure (red curves), $\delta\alpha_0^2$ is significantly increased and the pretransitional phenomena are markedly enhanced compared to the sham exposed membrane (black curves). Moreover, the transition region is broader and the transition point is shifted to a higher value (Figure 4).

Why is a much lower thermal energy required to create local area fluctuations in the presence of the radiation? A possible answer is that the radiation brings the membrane in a non-thermalized excited state, related to some structural change in the polar

headgroup region of the membrane bilayer, as proved by the $\Delta\nu_Q$ reduction in the exposed samples. This effect is clearly opposite to a thermal increase upon which an increase of the quadrupole splitting (water ordering increase) would occur (Figure 1). Therefore, the electromagnetic energy absorbed by the membrane is not thermalized.

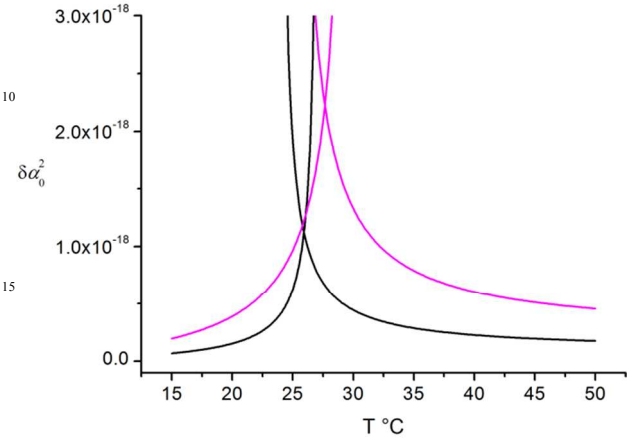

Fig. 4 Strength of the order parameter fluctuations, $\delta\alpha_0^2$, as a function of temperature for the sham (black curve) and millimeter waves exposed membrane sample (red curve). The precritical behavior of the membrane is greatly enhanced in the presence of the radiation and this causes an upward shift of the transition point and a broadening of the transition region.

5. Microscopic interpretation

5.1 Exposure time-dependent effect

As already observed in Figure 3, a significant decrease of the heavy water quadrupole splitting occurs only under long term exposure conditions (several hours). If the membrane is exposed far from the transition point, no phase transition is induced. However, a significant quadrupole splitting reduction occurs. Figure 5 shows the dependence of $\Delta\nu_Q$ on the exposure time at 37 °C. Notably, the quadrupole splitting is constant during exposure until the time $t = t_0+\tau$, where τ is the exposure time required to see an effect. After this time $\Delta\nu_Q$ decreases very rapidly of ~25%. This means that a certain amount of energy needs to be accumulated in the system before having an effect on the membrane. Further exposure does not induce significant effects but keeps the membrane in the same state. After the generator is turned off, $\Delta\nu_Q$ relaxes back to its pre-exposure equilibrium value, indicating that the effect is reversible. The relaxation process occurs with a relatively fast initial kinetics, in which the splitting is quite totally recovered in the first half an hour. However, complete relaxation generally takes 2-3 hours. This suggests that some structural rearrangement of the bilayer is induced by the radiation.

Despite the accumulated energy is small compared to *kT* (Table 2), the radiation is able to induce a gradual molecular reorganization of the membrane that can also lead to the fluid-to-gel transition if exposure is performed close to Tm (Figure 3). Interestingly, the application of osmotic pressures with energies < *kT* is also able to induce the fluid-gel phase transition in MLVs.[49]

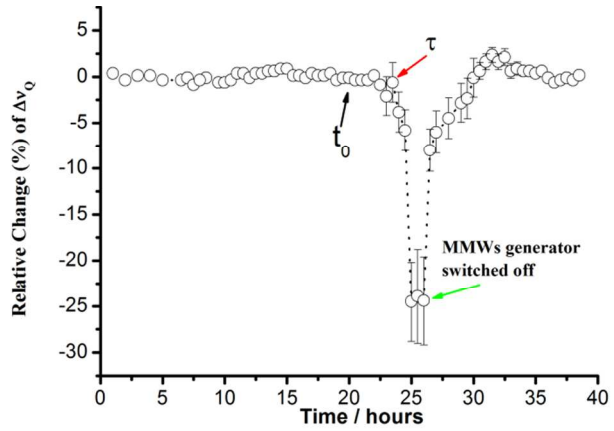

Fig. 5 Heavy water quadrupole splitting variation *vs.* time for DMPC/D2O MLV system with $n = 11$. For $0 < t \leq t_0$ sham exposure. For $t_0 < t \leq 26$ h MMWs exposure. For $t_0 > 26$ h post exposure. τ is a temporal threshold above which the MMWs-induced effect is observed. Error bars represent error means calculated from three independent experiments. Variability on the other points is contained within the symbols. Dot line was used merely to help the reader follow the trend of the points.

5.2 Hydration level-dependent effect

MMW interaction with the membrane must involve a coupling between some polarized states of the lipid bilayer and the MMW electric field. The primary mechanism of interaction takes into account the structure of the membrane components and their characteristic relaxation dynamics. Different temperature-dependent relaxation times in the range of microwave frequencies (10^{-7} to 10^{-12} s),[42] have been measured in membrane systems. Among all, local motions of water molecules have relaxation frequencies in the range $0.1\text{-}9\times10^{-12}$ s[50-52]and more likely can interact with MMWs, while other dynamic processes, such as membrane area fluctuations and water diffusion are too slow to be considered.[42] A further coupling mechanism of the radiation with the membrane can be due to the local dipole fluctuations of the C-H bonds (10^{-10}-10^{-11} s).[53] However, due to the large dielectric permittivity of water at these frequencies,[54] the predominant role is played by the interaction between its permanent dipole moment and radiation field.

It has been shown that water bound to phosphocholine membranes exhibits a variety of dielectric relaxation dynamics in the micorwave frequencies range (10^{-12} s).[55, 56] The fractions of the different types of bound water depend on the water/lipid mole ratio (n_w) as well as on T.[55] These THz time-domain spectroscopy studies also suggest that water molecules with different relaxation dynamics occupy different regions of the polar phosphocholine headgroups, in agreement with recent molecular dynamic simulations.[52] In addition, it was shown that the phosphocholine group changes its mean orientation with respect to the bilayer normal assuming increasing tilted conformations as the temperature and/or n_w decreases.[51]This supports the hypothesis that a redistribution of bound water, i.e., a change in the water partitioning (with different dielectric behaviour), is associated to a change in the headgroup mean orientation. In addition, upon cooling from the fluid phase toward the main phase transition temperature, multibilayer phosphocholine membranes exhibit the swelling phenomenon, i.e. an anomalous increase of the lamellar

repeat distance (larger than 5 Å).[37, 40, 41] Membrane swelling is due to an increase of the interbilayer water thickness, indicating that the ordering and/or the state of bound water is markedly affected by a temperature change and that water is pushed out from the most internal layers of the polar interface (carbonyl-phosphate region) toward the choline moiety. This can only occurs if a significant change of the phospholipid headgroup conformation is achieved on cooling the system.

Also, the response of the membrane to MMWs, measured as change of the quadrupole splitting of heavy water, depends on the hydration level of the membrane, increasing with the water/lipid mole ratio.[29] In equation (1) the quadrupole splitting is affected by the distribution of water among the various binding sites along the phospholipid group. A model describing such dependence has been proposed by Westlund and collaborators.[51, 57] This model explains for the evolution of ^{2}H (water) and ^{14}N (choline group) NMR quadrupole interactions and the typical relaxation times of the magnetization by considering the variation of water distribution among two interfacial regions. These two regions have been identified as the phosphate and the choline headgroup binding sites, and have local water orientational order parameter of opposite sign. In this case, eq. (1) can be written again taking into account the contribution of bound water at these two interfacial regions:

$$\Delta\nu_Q = \frac{3}{4}\nu_Q\left|P_{B_-}S_{B_-} + P_{B_+}S_{B_+}\right| \quad (7)$$

with, $P_{B_-}S_{B_-} + P_{B_+}S_{B_+} = P_B S_B < 0$; $P_{B_-} + P_{B_+} = P_B$

where, S_{B-} and S_{B+} (-0.0372 and + 0.0120) are the orientational order parameters of water at the – (phosphate) and + (choline) interface regions. P_{B-} and P_{B+} are the mole fractions of bound water ($S_B \neq 0$) in the corresponding binding sites and $P_B = n_B/(n_B+n_F)$, where n_B and n_F are the moles of bound and free water per mole of lipid, respectively.

Equation 7 shows that the quadrupole splitting of heavy water is very sensitive to changes in the relative populations of bound water at the two sites. A small increase of the fraction of water at the choline site, for instance, causes a net decrease of the splitting.[51, 57] The model gives a good interpretation of the temperature dependence of the quadrupole splitting, as a temperature change induces a variation in the water populations at the phosphate and choline sites. This is valid even when all the water molecules are bound to the polar groups (P_B = 1), i.e., in the hydration regime occurring for $n_w < 14$.[50, 58]

The dependence of the quadrupole splitting reduction on the water/lipid mole ratio suggests that: i. MMWs directly interact with bound water and ii. this interaction affects the water partitioning at the polar heads. According to eq. (7), the reduction of the quadrupole splitting during exposure, corresponds to a displacement of water from the phosphate to the choline site.

The equilibrium exchange reaction between water at the two sites of the phosphocholine group can be written as:

$$H_2O_{(b_-)} \xleftrightarrow{K} H_2O_{(b_+)} \quad (8)$$

The Gibbs free energy change for this reaction before and after exposure are, respectively:

$$\Delta G_0 = -RT\ln K \quad (9)$$

$$\Delta G_{(MMW)} = \Delta G_0 + \varepsilon = -RT\ln K_{MMW} \quad (10)$$

where, K and K_{MMW} are the respective equilibrium thermodynamic constants at temperature T:

$$K = \frac{p_{B_+}}{p_{B_-}} \quad (11)$$

$$K_{MMW} = \frac{p_{B_+,MMW} + \chi}{p_{B_-,MMW} - \chi} \quad (12)$$

where, χ represents the change in the fraction of water molecules. Assuming that the MMW energy is transformed into chemical potential energy, ε is the "extra chemical potential energy" provided to the system by the radiation and is given by:

$$\varepsilon = RT\ln\frac{K}{K_{MMW}} \quad (13)$$

K and K_{MMW} can be calculated from the experimental quadrupole splitting data before ($\Delta\nu_Q$) and after exposure ($\Delta\nu_{Q,MMW}$):

$$\Delta\nu_Q = \frac{3}{4}\nu_Q\left|P_{B_-}S_{B_-} + P_{B_+}S_{B_+}\right| \quad (14)$$

$$\Delta\nu_{Q,MMW} = \frac{3}{4}\nu_Q\left|P_{B_+,MW}S_{B_+} + (1-P_{B_+,MW})S_{B_-}\right| \quad (15)$$

$$P_{B_+,MW} = P_{B_+} + \chi \quad (16)$$

From the ratio $\frac{\Delta\nu_Q}{\Delta\nu_{Q,MW}}$ we have:

$$\chi = \frac{\Delta\nu_{Q,MW} - \Delta\nu_Q}{\Delta\nu_Q(S_{B+} + S_{B-})}\left[P_{B+}(S_{B+} + S_{B-}) - S_{B-}\right] \quad (17)$$

and, from eq. (11)-(12):

$$K = \frac{1-P_{B+}}{P_{B+}} \quad (18)$$

$$K_{MMW} = \frac{1-P_{B+}-\chi}{P_{B+}+\chi} \quad (19)$$

Table 4 reports the thermodynamic data relative to three exposure regimes where only the water/lipid mole ratio (n_w) has been changed. Taking into account the dosimetry data (Table 2) and that the typical sample weight was 60 mg, we can roughly estimate that that average power absorbed by the whole sample at 74 GHz is about 1 μW. Actually, this value is underestimated due to the simplified model of the scenario used in the dosimetric simulation that does not take into account the complex NMR probe architecture (Supplementary Fig. 1).

Table 4 Thermodynamic data

n_w	$\Delta\nu_Q$	$\Delta\nu_{Q,MMW}$	P_{B+}	χ	K	K_{MMW}	ε (kJ/mol)
7	605 (1)	558 (2)	0.6816 (0.0002)	0.0058 (0.0002)	0.467 (0.004)	0.4548 (0.002)	0.069 (0.002)
9	550 (2)	482 (2)	0.6884 (0.0004)	0.0085 (0.0006)	0.453 (0.004)	0.4352 (0.002)	0.102 (0.002)
11	406 (3)	307 (4)	0.7061 (0.0008)	0.0122 (0.0004)	0.416 (0.002)	0.3922 (0.002)	0.153 (0.001)

However, we can roughly estimate the average energy absorbed per mole of sample at this frequency, assuming that the electromagnetic energy is absorbed by water in the exchange process (8). With a water content of about 30% weight, the molar power absorbed by water is about 1 mW. Furthermore, assuming that the energy absorbed by the membrane accumulates with time, after 4 h of exposure we have that the accumulated energy is about 0.01 kJ/mol at 74 GHz. The overall molar energy absorbed by the sample is the sum of the molar energy absorbed at each frequency in the exposure band (53-78 GHz). Even if we have not estimated this value, we can say that it is larger than 0.01 kJ/mol. Therefore, the accumulated energy is expected to be close to the energy needed to shift the chemical equilibrium of bound water between the phosphate and the choline sites.

Conclusions

In conclusion, MMW exposure at very low SAR (14 mW/kg), directly interacts with the membrane via the coupling to the fast local relaxation processes of bound water molecules. The absorbed electromagnetic energy (< kT), does not cause thermal effects. In contrast, it brings the membrane into an excited state with a significant increase of the precritical thermal behavior of the membrane that causes a shift of the phase transition from a weakly first order to a pseudo-second order process. On a microscopic level this effect is induced by a redistribution of water molecules among the binding sites of the interfacial region. This mechanism may explain the high sensitivity of DMPC multilamellar vesicles to millimeter waves near the membrane main phase transition point and may provide a theoretical framework for several biological effects of millimeter waves for which nonthermal mechanisms have been claimed.[1, 4, 12, 21]

Notes and references

[a] *Department of Chemistry and Chemical Technologies, University of Calabria, Arcavacata di Rende (CS),Italy. Fax: +390984492041; Tel: +390984492117; E-mail: amerigo.beneduci@unical.it*
[b] *Consortium TEBAID c/o Department of Chemistry and Chemical Technologies, University of Calabria, Arcavacata di Rende (CS)*
[c] *CNR-Institute for the Electromagnetic Sensing of the Environment (IREA), Via Diocleziano 328, 80124, Napoli*
[d] *Department of Physics, University of Naples, Via Cintia - Complesso Monte S. Angelo, 80126, Napoli*

† Electronic Supplementary Information (ESI) available: Fig. S1 displaying the model of the MMWs applicator for dosimetric simulation. See DOI: 10.1039/b000000x/

1. M. Zhadobov, N. Chahat, R. Sauleau, C. Le Quement and Y. Le Drean, *International Journal of Microwave and Wireless Technologies*, 2011, **3**, 237-247.
2. T. Kleine-Ostmann and T. Nagatsuma, *J Infrared Milli Terahz Waves*, 2011, **32**, 143-171.
3. A. Beneduci, *Cell Biochem Biophys*, 2009, **55**, 25-32.
4. A. G. Pakhomov, Y. Akyel, O. N. Pakhomova, B. E. Stuck and M. R. Murphy, *Bioelectromagnetics*, 1998, **19**, 393-413.
5. I. Y. Belyaev, *Microwave Review*, 2005, **11**, 13-29.
6. A. G. Pakhomov and P. R. Murthy, *Plasma Science, IEEE Transactions on*, 2000, **28**, 34-40.
7. M. A. Rojavin, A. A. Radzievsky, A. Cowan and M. C. Ziskin, *Int J Radiat Biol*, 2000, **76**, 575-579.
8. M. Rojavin and M. Ziskin, *QJM*, 1998, **91**, 57-66.
9. A. A. Radzievsky, O. V. Gordiienko, I. Szabo, S. I. Alekseev and M. C. Ziskin, *Bioelectromagnetics*, 2004, **25**, 466-473.
10. R. K. Adair, *Bioelectromagnetics*, 2003, **24**, 39-48.
11. C. Le Quément, C. Nicolas Nicolaz, M. Zhadobov, F. Desmots, R. Sauleau, M. Aubry, D. Michel and Y. Le Dréan, *Bioelectromagnetics*, 2012, **33**, 147-158.
12. A. Beneduci, *Bioelectrochemistry Research Developments*, 2008, **2**, 35-80.
13. S. Sun, I. Titushkin, J. Varner and M. Cho, *Journal of radiation research*, 2012, **53**, 159-167.
14. V. Pikov, X. Arakaki, M. Harrington, S. E. Fraser and P. H. Siegel, *Journal of neural engineering*, 2010, **7**, 045003.
15. A. Deghoyan, A. Heqimyan, A. Nikoghosyan, E. Dadasyan and S. Ayrapetyan, *Electromagnetic biology and medicine*, 2012, **31**, 132-142.
16. H. Fröhlich, *Biological coherence and response to external stimuli*, Springer-Verlag, 1988.
17. J. R. Reimers, L. K. McKemmish, R. H. McKenzie, A. E. Mark and N. S. Hush, *Proceedings of the National Academy of Sciences*, 2009, **106**, 4219-4224.
18. A. Beneduci and G. Chidichimo, *J Infrared Milli Terahz Waves*, 2012, **33**, 529-547.
19. O. P. Gandhi, M. J. Hagmann, D. W. Hill, L. M. Partlow and L. Bush, *Bioelectromagnetics*, 1980, **1**, 285-298.
20. M. Zhadobov, R. Sauleau, V. Vie, M. Himdi, L. Le Coq and D. Thouroude, *Microwave Theory and Techniques, IEEE Transactions on*, 2006, **54**, 2534-2542.
21. A. Ramundo-Orlando, *J Infrared Milli Terahz Waves*, 2010, **31**, 1400-1411.
22. A. Beneduci, L. Filippelli, K. Cosentino, M. L. Calabrese, R. Massa and G. Chidichimo, *Bioelectrochemistry*, 2012, **84**, 18-24.
23. K. Cosentino, A. Beneduci, A. Ramundo-Orlando and G. Chidichimo, *Journal of Biological Physics*, 2013, 1-16.
24. A. Ramundo-Orlando, G. Longo, M. Cappelli, M. Girasole, L. Tarricone, A. Beneduci and R. Massa, *Biochimica et Biophysica Acta (BBA)-Biomembranes*, 2009, **1788**, 1497-1507.

25. S. Espinosa, N. Asproulis and D. Drikakis, *Microfluidics and Nanofluidics*, 2013, 1-10.
26. D. Drikakis, J. Lechuga and S. Pal, *Journal of Computational and Theoretical Nanoscience*, 2009, **6**, 1437-1442.
27. G. Nair, J. F. Gargiuli, N. R. Shiju, Z. Rong, E. Shapiro, D. Drikakis and P. Vadgama, *ChemBioChem*, 2006, **7**, 1683-1689.
28. J. Gargiuli, E. Shapiro, H. Gulhane, G. Nair, D. Drikakis and P. Vadgama, *Journal of membrane science*, 2006, **282**, 257-265.
29. A. Beneduci, K. Cosentino and G. Chidichimo, *Materials*, 2013, **6**, 2701-2712.
30. J. Jin, in *Electromagnetic analysis and design in magnetic resonance imaging*, CRC press, Florida, 1998, pp. 224-226.
31. M. L. Calabrese, G. d'Ambrosio, R. Massa and G. Petraglia, *Microwave Theory and Techniques, IEEE Transactions on*, 2006, **54**, 2256-2264.
32. J. Pope, L. Walker, B. Cornell and G. Francis, *Biophysical journal*, 1981, **35**, 509-520.
33. R. L. Smith and E. Oldfield, *Science*, 1984, **225**, 280-288.
34. J. H. Davis, *Biochimica et Biophysica Acta (BBA) - Reviews on Biomembranes*, 1983, **737**, 117-171.
35. G. Chidichimo, A. Golemme and J. W. Doane, *The Journal of Chemical Physics*, 1985, **82**, 4369-4375.
36. J. F. Nagle, H. I. Petrache, N. Gouliaev, S. Tristram-Nagle, Y. Liu, R. M. Suter and K. Gawrisch, *Physical Review E*, 1998, **58**, 7769.
37. D. Papahadjopoulos, K. Jacobson, S. Nir and I. Isac, *Biochimica et Biophysica Acta (BBA)-Biomembranes*, 1973, **311**, 330-348.
38. S. Doniach, *The Journal of Chemical Physics*, 1978, **68**, 4912-4916.
39. J. Nagle and H. Scott Jr, *Biochimica et Biophysica Acta (BBA)-Biomembranes*, 1978, **513**, 236-243.
40. B. Stidder, G. Fragneto, R. Cubitt, A. V. Hughes and S. J. Roser, *Langmuir*, 2005, **21**, 8703-8710.
41. H. Seto, N. Yamada, M. Nagao, M. Hishida and T. Takeda, *The European Physical Journal E*, 2008, **26**, 217-223.
42. F. Jähnig, *Biophysical journal*, 1981, **36**, 329-345.
43. F. Jähnig, *Biophysical journal*, 1981, **36**, 347-357.
44. J. Ipsen, K. Jørgensen and O. Mouritsen, *Biophysical journal*, 1990, **58**, 1099-1107.
45. M. H. Hawton and J. W. Doane, *Biophysical journal*, 1987, **52**, 401-404.
46. *IEEE Std C95.1-2005 (Revision of IEEE Std C95.1-1991)*, 2006, 0_1-238.
47. J. L. Finney, *Journal of Molecular Liquids*, 2001, **90**, 303-312.
48. F. Frank, *Water*, Revised 1st edition edn., The royal society of chemistry, Cambridge, London, 1983.
49. V. A. Parsegian, R. P. Rand, N. L. Fuller and D. C. Rau, *Methods in enzymology*, 1986, **127**, 400-416.
50. B. W. Koenig, H. H. Strey and K. Gawrisch, *Biophysical journal*, 1997, **73**, 1954-1966.
51. T. Sparrman and P.-O. Westlund, *Physical Chemistry Chemical Physics*, 2003, **5**, 2114-2121.
52. K. Åman, E. Lindahl, O. Edholm, P. Håkansson and P.-O. Westlund, *Biophysical journal*, 2003, **84**, 102-115.
53. J. D. Bond and N. C. Wyeth, *The Journal of chemical physics*, 1986, **85**, 7377-7379.
54. A. Beneduci, *Journal of Molecular Liquids*, 2008, **138**, 55-60.
55. K. J. Tielrooij, D. Paparo, L. Piatkowski, H. J. Bakker and M. Bonn, *Biophysical journal*, 2009, **97**, 2484-2492.
56. D. Paparo, K.J. Tielrooij, H.J. Bakker and M. Bonn, *Molecular Crystals and Liquid Crystals*, 2009, **500**, 108-117.
57. P.-O. Westlund, *The Journal of Physical Chemistry B*, 2000, **104**, 6059-6064.
58. C. Faure, L. Bonakdar and E. J. Dufourc, *FEBS letters*, 1997, **405**, 263-266.